



Rosli, R. and Norman, R. and Atlar, M. (2016) Experimental investigations of the Hydro-Spinna turbine performance. Renewable Energy, 99. 1227–1234. ISSN 0960-1481 , <http://dx.doi.org/10.1016/j.renene.2016.08.034>

This version is available at <https://strathprints.strath.ac.uk/59420/>

Strathprints is designed to allow users to access the research output of the University of Strathclyde. Unless otherwise explicitly stated on the manuscript, Copyright © and Moral Rights for the papers on this site are retained by the individual authors and/or other copyright owners. Please check the manuscript for details of any other licences that may have been applied. You may not engage in further distribution of the material for any profitmaking activities or any commercial gain. You may freely distribute both the url (<https://strathprints.strath.ac.uk/>) and the content of this paper for research or private study, educational, or not-for-profit purposes without prior permission or charge.

Any correspondence concerning this service should be sent to the Strathprints administrator: strathprints@strath.ac.uk

1

2

Title: Experimental Investigations of the Hydro-Spinna Turbine Performance

3

4

5

6

7

R. Rosli*, R. Norman and M. Atlar

8

9

10

School of Marine Science and Technology

11

Armstrong Building

12

Newcastle University

13

Newcastle upon Tyne

14

NE1 7RU

15

United Kingdom

16

17

18

19

20 Keywords: tidal current, tidal turbine, turbine design, horizontal axis, power,
21 performance

22

23 * Corresponding Author: Roslyna Rosli h.r.haji-rosli@newcastle.ac.uk

24

25

26 Abstract

27 A unique tidal turbine, "Hydro-Spinna", is introduced. The Hydro-Spinna consists of
28 three cardioidal blades spiralling around a common horizontal shaft. A 500 mm
29 diameter model was manufactured and its performance investigated in the towing tank
30 facility of Newcastle University. The main objective of these experiments was to
31 investigate the hydrodynamic efficiency of Hydro-Spinna with a view to improving the
32 design by collecting data for use in numerical optimisation. Considering its flexible
33 operating characteristics the model turbine was tested at different immersion depths
34 and in the half-submerged condition. The power coefficient of the turbine reached a
35 value of almost 0.3 at a tip speed ratio of 2.2 in the fully submerged condition. The
36 turbine had a higher power coefficient in shallow immersion and half submerged
37 condition. The drag coefficient on the whole system decreased with increasing TSR
38 contrary to conventional turbines. The turbine was observed to start rotating at low
39 flow velocities, down to 0.15 m/s. In the study, although the turbine presents a
40 relatively low power coefficient compared to that of competitive turbines, its unique
41 adaptability of immersion depth, including the partially submerged condition, low
42 starting flow velocity and rotational speed offer an interesting prospect for a range of
43 applications.

44
45
46
47
48
49
50
51
52
53
54
55
56
57
58

59 1. Introduction

60 Persisting environmental concerns along with the volatile nature of the fossil fuel
61 economy reinforce the need to search further for sustainable alternative energy
62 resources. The world's oceans which cover 71% of the earth's surface offer an array
63 of marine energy opportunities with the potential to be exploited. In the UK alone, wave
64 and tidal energy resources have been identified as being able to meet 20% of the
65 energy requirements [1]. Tidal energy offers more opportunities due to its high
66 predictability; unlike the less predictable waves, tides result from the regular
67 gravitational interaction between the earth and the moon.

68 The traditional way of harvesting energy from tides is by means of a tidal barrage,
69 exploiting the potential head available in the water and operating similar to a
70 hydropower plant [2]. An alternative method is to extract the kinetic energy from the
71 flow using tidal current turbines. The wind energy industry has been successful in
72 establishing the generic design of horizontal axis turbine as the optimal configuration
73 for energy extraction. Due to the similarity of wind and tidal flow, both being fluids, the
74 horizontal axis turbine concept is the most commonly adopted format in the tidal
75 energy industry.

76 A horizontal axis turbine is used to extract energy from the kinetic component of a
77 moving fluid and the design of the turbine blade plays a very important role in the
78 efficiency of the turbine. Tidal ranges and velocities vary depending on geographical
79 location, land and seabed topography, with a peak velocity between 2 to 3 m/s
80 considered as an economically viable site for extracting tidal energy [3]. Typically at
81 such a site the tidal velocity ranges between 2 to 2.5 m/s during neap tide and 3.5 to
82 4 m/s during spring tide [4]. At certain locations, tidal velocities can reach up to 5 m/s
83 as the tidal flow is amplified by geographical constraints such as narrow straits or
84 headlands [5].

85 The maximum limit on the power that can be extracted from the fluid flow is 59%
86 according to the Betz Theory [6]. The power available in the fluid flow is shown in
87 equation (1).

88

$$89 P_{av} = \frac{1}{2} \rho A U^3 \quad (1)$$

90 where ρ is the density of the fluid, A is the swept area of the turbine and U is the flow
91 velocity.

92 Wind turbines require relatively large diameters to extract the energy effectively
93 from the flow however, the density of water is approximately 800 times higher than
94 that of air, hence tidal turbines would have significantly smaller diameters for the same
95 power rating. The power available in the flow is proportional to the velocity cubed, as
96 shown in equation (1), so a fluctuating flow velocity will greatly affect the power.
97 However, the tidal velocity is more predictable and fluctuates less compared to wind
98 velocity. The velocity of a tidal stream is lower than the velocity of wind, therefore tidal
99 turbines operate at slower rotational speeds as the energy content is greater in a tidal
100 flow than in wind, a tidal turbine is subjected to higher loading than a wind turbine
101 which requires a robust system.

102 Operation of tidal turbines can generate noise that may disturb the acoustic balance
103 of the natural environment they are deployed in [7]. In the case where they are installed
104 near the seabed, in shallow waters, they may increase the risk of scouring as reported
105 in [8]. In addition, tidal turbines are prone to cavitation, that may be increased by the
106 action of wave particle motions, causing the turbine blade to erode as well as radiating
107 noise hence compromising its hydrodynamic integrity and further impacting on the
108 marine environment [7,8]. On a similar note free surface effects due to waves and the
109 turbine's own operation affect its energy production [9–11].

110 Most established tidal current devices are based on the conventional horizontal axis
111 turbine generally adopted in the wind industry. Established horizontal axis tidal current
112 energy, such as SeaGen [12] put the emphasis on the reliability and adaptability of
113 such a design for tidal energy. Various other devices are also being tested at the
114 European Marine Energy Centre (EMEC) reflecting the steady progress in the marine
115 energy industry in the region. A significant amount of work has been done to study the
116 performance of tidal current turbines at various working and flow conditions as well as
117 the wake profiles [9,13–15]. Vertical axis tidal turbines and other unconventional tidal
118 current devices have also been developed and investigated to harness the energy
119 from tides [1,16–19].

120 A working novel marine current turbine design is presented in this paper including
121 an experimental investigation into the power extraction capability of this turbine. The

122 “Hydro-Spinna”, which is the name given to the device by its inventor based on his
123 wind spinner activity and observation [27], offers an innovative horizontal axis concept
124 design for the tidal current energy industry. The unique design of the Hydro-Spinna is
125 presented in Section 2 including its geometrical definition through analytical equations.
126 The experimental set-up and tests for the evaluation of the power extraction
127 performance are presented in Section 3. The performance results are investigated at
128 different immersion depths over a range of operating tip speed ratio (TSR) and results
129 are discussed in Section 4. Finally, Section 5 reports on the conclusions of the study.

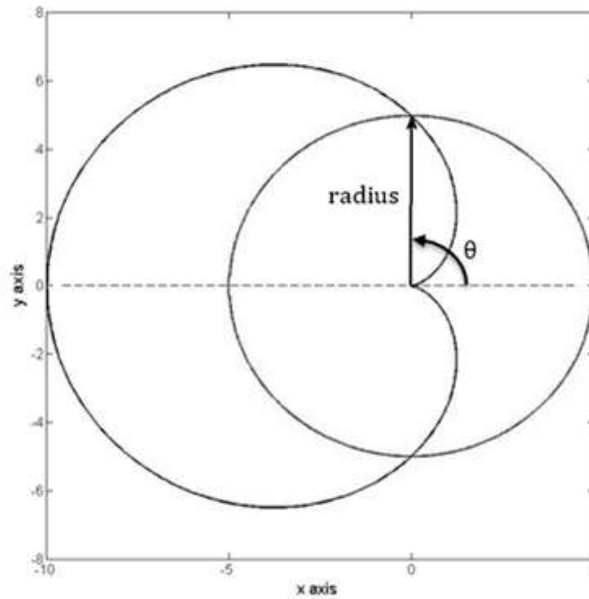
130

131 **2. Hydro-Spinna turbine**

132 *2.1. Turbine design*

133 The Hydro-Spinna is a three cardioidal helicoidal bladed turbine which extracts energy
134 from the tidal stream by aligning itself in the direction of the flow. A cardioid is a
135 geometrical shape that follows the polar x-y coordinates of a circle. However, in the
136 case of a circle where the radius is constant at every swept angle θ , the radius of the
137 cardioid varies with angle, as presented in Figure 1, and is defined as $r = a(1 - \cos \theta)$
138 where a is the scaling factor and $0 < \theta < 2\pi$. The plan form of the blade in the x-y
139 direction is formed by creating two concentric cardioids as shown in Figure 2.

140 Two generations of the Hydro-Spinna turbine have previously been designed,
141 maintaining the basic cardioid leading edge design of the blade [20,21]. The first
142 generation developed has a cardioid leading and trailing edge with equal chord length
143 throughout the blade circumference while the second generation exhibits a circular
144 trailing edge profile. The third generation turbine investigated in this paper is a
145 modified version of the first generation and is further defined in the following.



146

147 Figure 1. The basic cardioid geometry and comparison of the cardioid shape (scaling
 148 factor $a = 5$) with a circle of radius = 5 for $0 < \theta < 2\pi$.

149

150 The third generation turbine has cardioidal leading and trailing edges. The design
 151 of the turbine is developed in a mathematical form for simplicity of design and
 152 construction. The scaling factor ratio of the trailing to the leading cardioid is 1.5. The
 153 offset of the leading and trailing cardioid surfaces are given in equations (2 – 4), while
 154 pitch angle, β , of the surface at any radius is given by equation (5).

155

$$156 \quad x = a(1 - \cos \theta) \cos \theta \quad (2)$$

$$157 \quad y = a(1 - \cos \theta) \sin \theta \quad (3)$$

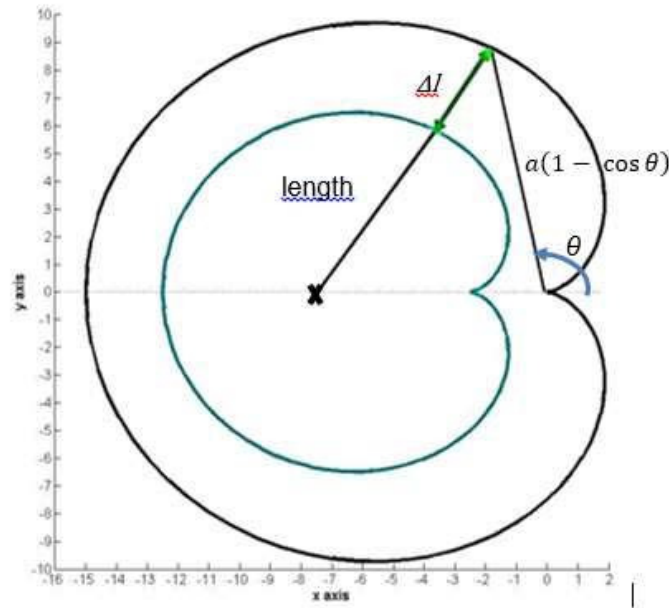
$$158 \quad z = p\theta \quad (4)$$

$$159 \quad \beta = \tan^{-1} \left[\frac{\Delta Z}{\Delta l} \right] \quad (5)$$

160

161 where a is the cardioid scaling factor, θ is the swept angle, p is the pitch length of the
 162 turbine, ΔZ is the axial distance between the trailing and leading edge, and Δl is the
 163 chord length,

164



165

166 Figure 2. The planform view of a Hydro-Spinna blade. The chord length of the blade,
 167 Δl , is the length from the leading to trailing edge at the same angle θ from the
 168 designated centre \mathbf{x} .

169

170 As each blade is spiraled around the hub along its longitudinal axis (z-axis), the
 171 blade meets the hub at two points, named the upstream and downstream end. The
 172 pitch length of the turbine (p) is the distance between the upstream and downstream
 173 end of the hub where the blade completes one helicoidal cycle in the axial fluid flow
 174 direction along the z- axis. The hub radius of the third generation device is 20% of the
 175 turbine diameter as illustrated in Figure 3.

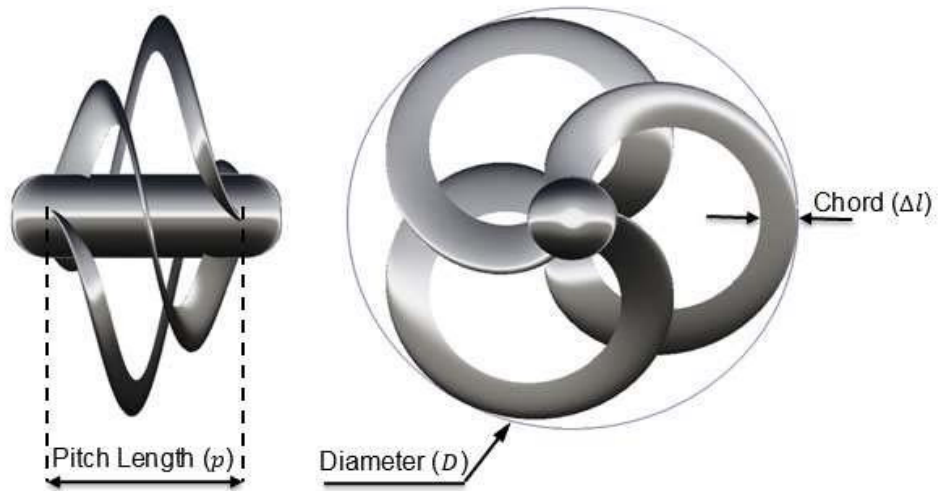
176

177 2.2. Hydro-Spinna model

178 The Hydro-Spinna has a unique design and key parameters need to be clearly
 179 defined. The diameter of the turbine (D) is defined as the diameter of the cross
 180 sectional area swept by the turbine. The pitch length (p) and chord (Δl) as described
 181 earlier are shown in Figure 3 while the blade shape for the third generation device
 182 used an aerodynamic NACA0015 profile cross-section for its symmetrical and thick
 183 profile that will give structural stability to the blade.

184

185



186
187
188

Figure 3. Hydro-Spinna parameters defined.

189 The Hydro-Spinna model tested in the towing tank has a diameter of 500mm with a
190 pitch to diameter ratio of 0.42 and hub diameter of 100mm. The model was
191 manufactured from polymers using a 3-D printer as shown in Figure 4. The radial
192 distribution of the blade section details are given in Table 1:

193



194
195
196
197

Figure 4. The 3-D printed Hydro-Spinna turbine

198 Table 1. Specification of the Hydro-Spinna model with the pitch angle and chord
 199 length defined at each cardioid radius.

Cardioid Angle, θ	Cardioid Radii(mm)	Pitch Angle ($^{\circ}$) β	Chord (mm) Δl
0	0	50.2	65.1
30	16.7	41.8	62.5
60	62.5	31.1	64.4
90	125.0	23.0	64.0
120	187.5	16.8	57.6
150	233.3	10.1	47.3
180	250.0	0	41.7
210	233.3	-10.1	47.3
240	187.5	-16.8	57.6
270	125.0	-23.0	64.0
300	62.5	-31.1	64.4
330	16.7	-41.8	62.5
360	0	-50.2	65.1

200
201

202 3. Experimental set up and tests

203 3.1. Test facility and limitations

204 Tests were carried out in the Towing Tank facility at Newcastle University. The tank
 205 has the following dimensions while its further details can be found in [22]:

206

207	Tank length	37 m
208	Width	3.7 m
209	Depth	1.25 m
210	Maximum carriage velocity	3 m/s

211

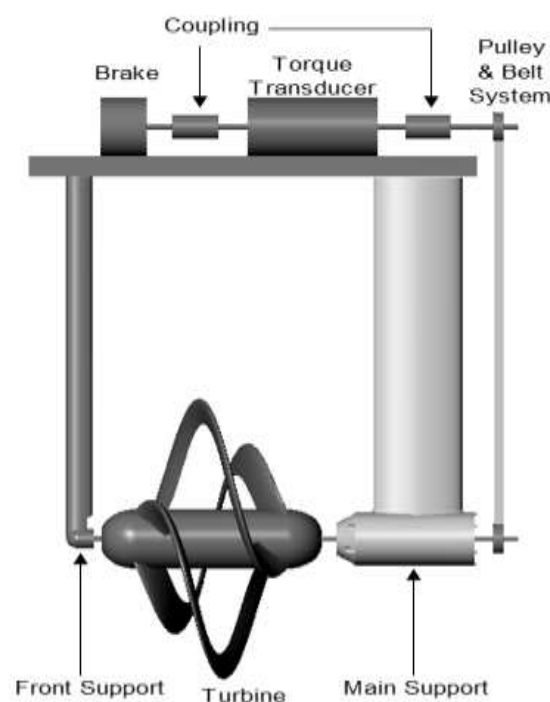
212 Although the towing carriage can be driven up to a maximum speed of 3 m/s, the
 213 rotational speed of the turbine was regulated by a 1 Nm Magtrol HB-140M-2 magnetic
 214 brake . The turbine model therefore was tested up to a maximum carriage velocity of
 215 0.9 m/s including tests at 0.5 and 0.7 m/s. This was due to the limitation of the brake
 216 capacity of 1 Nm that was insufficient to control the turbine rotation for lower TSR at
 217 higher flow velocities. A full range of tip speed ratio tests was only obtained at the
 218 minimum carriage velocity of 0.5 m/s.

219

220 3.2. Test set up

221 The Hydro-Spinna was supported by a front and back (main) struts to distribute the
222 weight of the turbine as shown in Figure 5. The front strut was introduced to support
223 the weight of the turbine as well as to strengthen the entire assembly against the
224 unsteady effects of the thrust and torque on the blades. Mechanical power was
225 transmitted from the turbine via a pulley system to a shaft drive above the water level
226 attached to the carriage rig.

227



228

229 Figure 5. Illustration of the turbine set up for the towing tank test

230

231 As shown in Figures 5 and 6, the shaft drive was connected to the 1Nm rated brake
232 and a torque transducer to control the rotational speed of the turbine, and measure
233 the torque and rotational speed, respectively. The thrust on the turbine alone was not
234 measured. However, the overall turbine system was attached to a carriage equipped
235 with load cells to measure the total drag force of the turbine and both front and main
236 supports.

237 Experimental data was recorded every 0.01 seconds where 10 seconds of data
238 were taken giving a total of 1001 samples. A total of 3 runs were carried out for each

239 condition. The standard deviation and standard error with 95% confidence level for the
240 carriage velocity, turbine rotational speed and torque are defined in Table 2.

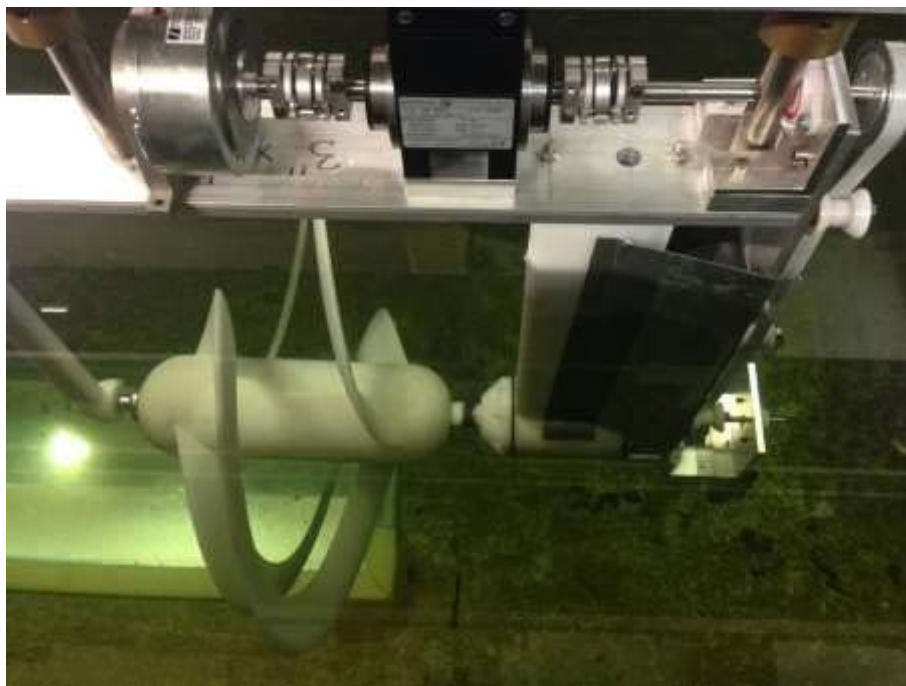
241

242 Table 2. Experiment data standard deviation and standard error

243

	Standard Deviation	Standard Error
Carriage Velocity (m/s)	0.13	± 0.008
Rotational Speed (rpm)	2.45	± 0.1
Torque (Nm)	0.02	± 0.001

244



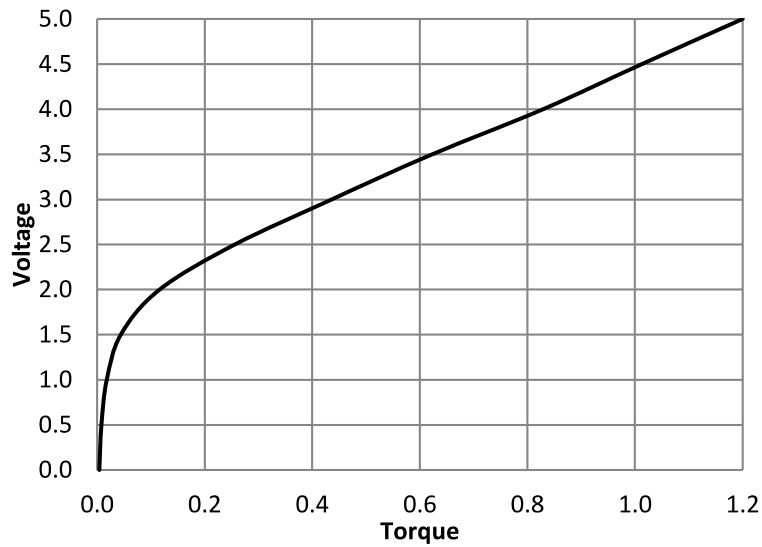
245

246 Figure 6. The Hydro-Spinna experimental set up in the towing tank facility.

247

248 3.3. Brake calibration

249 The hysteresis brake controlled the rotational speed of the turbine based on the
250 amount of voltage supplied. The voltage and current have a linear relationship and the
251 relationship of either to the resulting torque is linear above approximately 2.5V as
252 shown in Figure 7 below. Since it was easier to regulate the voltage than the current,
253 a control box with a trigger mechanism was used to regulate the voltage supplied to
254 the brake for each run. Hence, voltages were regulated between 2.5V and the
255 maximum voltage of 5V by increasing the voltage in each case.



257

258

259

260

Figure 7. The voltage and torque relationship of the hysteresis brake calibrated with increasing voltage.

261 *3.4. Towing tank tests*

262

263

264

The aim of the tests was to investigate the performance of the Hydro-Spinna turbine at four different depths of immersion. The range of immersions tested was as described in Table 3 and shown in Figure 8.

265

266

Table 3. Range of immersion depth of the towing tank test

267

Immersion Depth	Distance (turbine tip to water surface)
0.36D (submerged)	180 mm
0.2D (submerged)	100 mm
0.0D (submerged)	0 mm (Blade tip at the water surface)
-0.5D (partially submerged)	-250mm (half of the turbine is underwater)

268

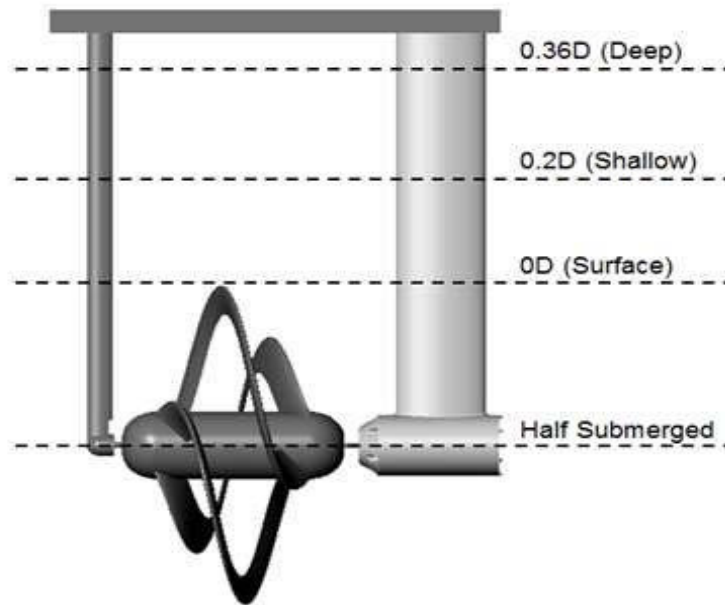
269

270

271

The water depth from the bottom of the tank to the shaft centre of the turbine was 470mm. At a turbine immersion level of 0.36D, the total water depth in the tank was

272 900mm. The depth of tip immersion was changed by draining the water out of the
 273 towing tank maintaining a constant level of water between the turbine and the bottom
 274 of the tank.
 275



276
 277 Figure 8. Illustration of different depth of immersion for the test
 278

279

280 4. Test results and analysis

281 4.1. Energy conversion theory

282 The power generated by the turbine is defined in the non-dimensional power
 283 coefficient. Similarly, the thrust coefficient describes the thrust experienced by the
 284 whole system as listed in equations (6-7). The performance of turbine is generally
 285 presented in plots represented by these coefficients against the tip speed ratios (TSR).
 286 TSR is defined as the ratio of the angular velocity at the blade tip to the axial flow
 287 velocity as given in equation (8).

288

289 Power Coefficient $C_P = \frac{Q\Omega}{0.5 \rho AU^3}$ (6)

290 Thrust Coefficient $C_T = \frac{T}{0.5 \rho AU^2}$ (7)

291 Tip Speed Ratio $TSR = \frac{R\Omega}{U}$ (8)

292

293

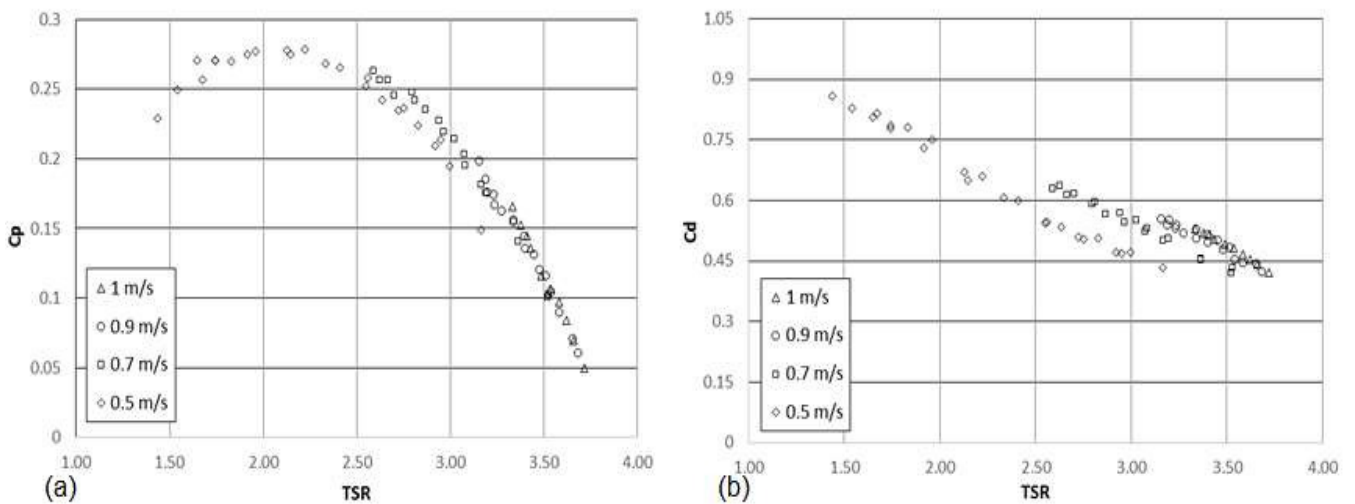
294 where ρ is the density of the fluid, R is the turbine radius, A is the swept area of the
295 turbine, U is the flow velocity, T is the thrust, Q is the torque and Ω is the angular
296 velocity.

297

298 4.2. Test results and discussions

299 The power coefficient of the turbine at fully submerged level of tip immersion 0.36D
300 is presented in Figure 9(a). The graph shows the limitation set by the 1Nm brake in
301 getting the full speed range for velocities higher than 0.5 m/s. The turbine produce a
302 maximum power coefficient of 0.275 at an optimal TSR of 2.2. The power performance
303 of the Hydro-Spinna is lower than conventional horizontal axis tidal turbines where a
304 contra-rotating turbine might typically generate a power coefficient of about 0.45
305 between TSR of 4 and 8 [23]. In another study conducted [9] the performance of the
306 800 mm diameter tidal turbine generated similar power coefficients with a maximum
307 of 0.46 at TSR of about 6.

308



309

310 Figure 9. Performance of the Hydro-Spinna (a) power coefficient and (b) drag
311 coefficient at flow velocities from 0.5 up to 1 m/s.

312

313 The range of the operational tip speed ratio of the Hydro-Spinna model is lower than
314 that of common horizontal axis turbines where operational tip speed ratio is up to a
315 maximum value of 12. The range of operation of the Hydro-Spinna reaches a

316 maximum of just below TSR = 4. Although this seems to be a major disadvantage at
317 the outset the higher blade efficiency may not be the most important criteria for tidal
318 turbines designed to operate for geographical areas with higher tide velocities. In
319 contrast, the low operational TSR range of the Hydro-Spinna indicates that the turbine
320 operates optimally at a much lower rotational speed compared to a conventional tidal
321 current turbine [14,24,25]. This will be an important advantage for removing the
322 possible risk of cavitation and hence associated erosion damage on the blade sections
323 as well as reducing the level of underwater radiated noise that could disturb the marine
324 environment.

325

326 It is also observed that the Hydro-Spinna does not require high fluid velocity to
327 overcome its starting torque where it takes a minimum flow of 0.15 m/s for the turbine
328 model to start operating. Even though the Hydro-Spinna doesn't extract as much
329 power as a conventional tidal turbine, its low start up flow velocity makes it operable
330 at speeds below those at which conventional turbines usually start generating. Hence,
331 it is capable of generating power over a longer duration than a conventional turbine.
332 In addition higher blade efficiency may not necessarily be the prime importance for
333 turbines operating in relatively high tidal velocities and designed based on the stall
334 regulation.

335

336 The drag of the whole system includes the thrust subjected on the turbine and the
337 supports by the fluid flow. The drag coefficient of the whole turbine system was
338 measured and is presented in Figure 9(b) and defined in equation (9).

339

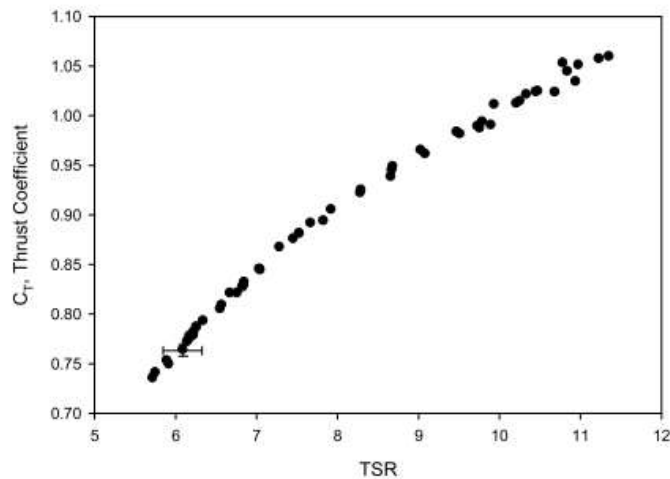
$$340 \quad C_D = \frac{D}{0.5\rho A_B U^2} \quad (9)$$

341

342 where D is the drag force and A_B is the projected area of the system perpendicular
343 to the flow direction.

344

345 The results show a decreasing trend in the drag coefficient and hence **thrust** as the
346 rotational speed of the turbine increases. The drag coefficient is the highest at the tip
347 speed ratio where the turbine starts to rotate and as the tip speed ratio increases, the
348 drag coefficient decreases.



350

351 Figure 10. Thrust coefficient profile for a NACA 63-618 three bladed horizontal
 352 axis turbine showing the increasing trend of the thrust coefficient with TSR [24].

353

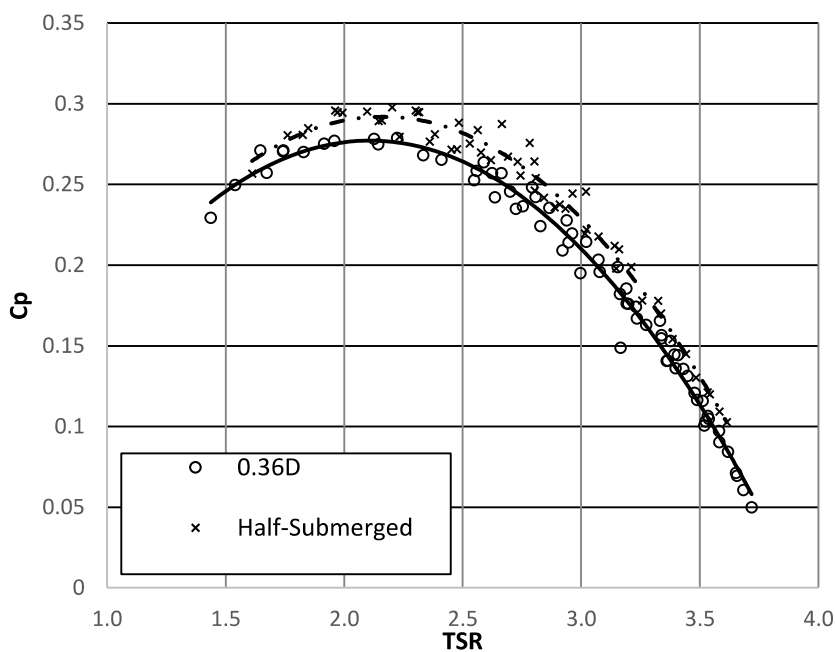
354 The decreasing drag coefficient of the Hydro-Spinna with increasing TSR (or
 355 reducing flow speed) demonstrates a contrasting observation in the thrust coefficient
 356 trend produced by other horizontal axis tidal current turbines. Generally, the thrust on
 357 the tidal turbine increases with the rotational speed as presented in other studies
 358 [9,24,26,27]. For comparison, the thrust coefficient on a common horizontal axis
 359 turbine is extracted from Luznik [24] and reproduced in Figure 10 but note that this
 360 turbine operates over a higher TSR range than the Hydro Spinna. The distinct drag
 361 coefficient profile of the Hydro-Spinna may be due to the nature of the turbine itself as
 362 it is extended in the axial dimension. The blade pitch angle in the front half of the
 363 turbine is positive, while the pitch angle of the rear half of the turbine is negative, where
 364 the direction of the resultant velocity seen by each half will be different. It is suggested
 365 that the trend is produced due to the interactions of the resultant forces on the blades
 366 of the Hydro-Spinna. The behaviour of the drag coefficient needs to be further
 367 investigated. The decreasing drag indicates a lower loading mooring system can be
 368 employed for the Hydro-Spinna turbine, which is likely to be a floating device, than the
 369 equivalent conventional device.

370

371 The performance of the turbine at 0.36 immersion level was compared against the
 372 half submerged performance as shown in Figure 11; the results present a unique
 373 finding in the performance of the turbine when the turbine is half submerged. At half

374 submerged condition the Hydro-Spinna was found to generate half the power of that
 375 at the 0.36D immersion level. However, the Hydro-Spinna is only extracting power
 376 from half of the turbine swept area hence the power coefficient is 5.5% higher at a
 377 TSR of 2.25 than when the turbine was fully immersed at 0.36D. Where in the former
 378 case, the power available in the flow is calculated only for the area of the turbine which
 379 is submerged in the water i.e. half of the turbine area. The power available in the air
 380 for the section of the turbine above the water level is assumed insignificant and its
 381 contribution neglected in the calculation.

382



383

384 Figure 11. Power coefficient of the Hydro-Spinna turbine at different flow velocity
 385 at deep immersion and half submerged condition

386

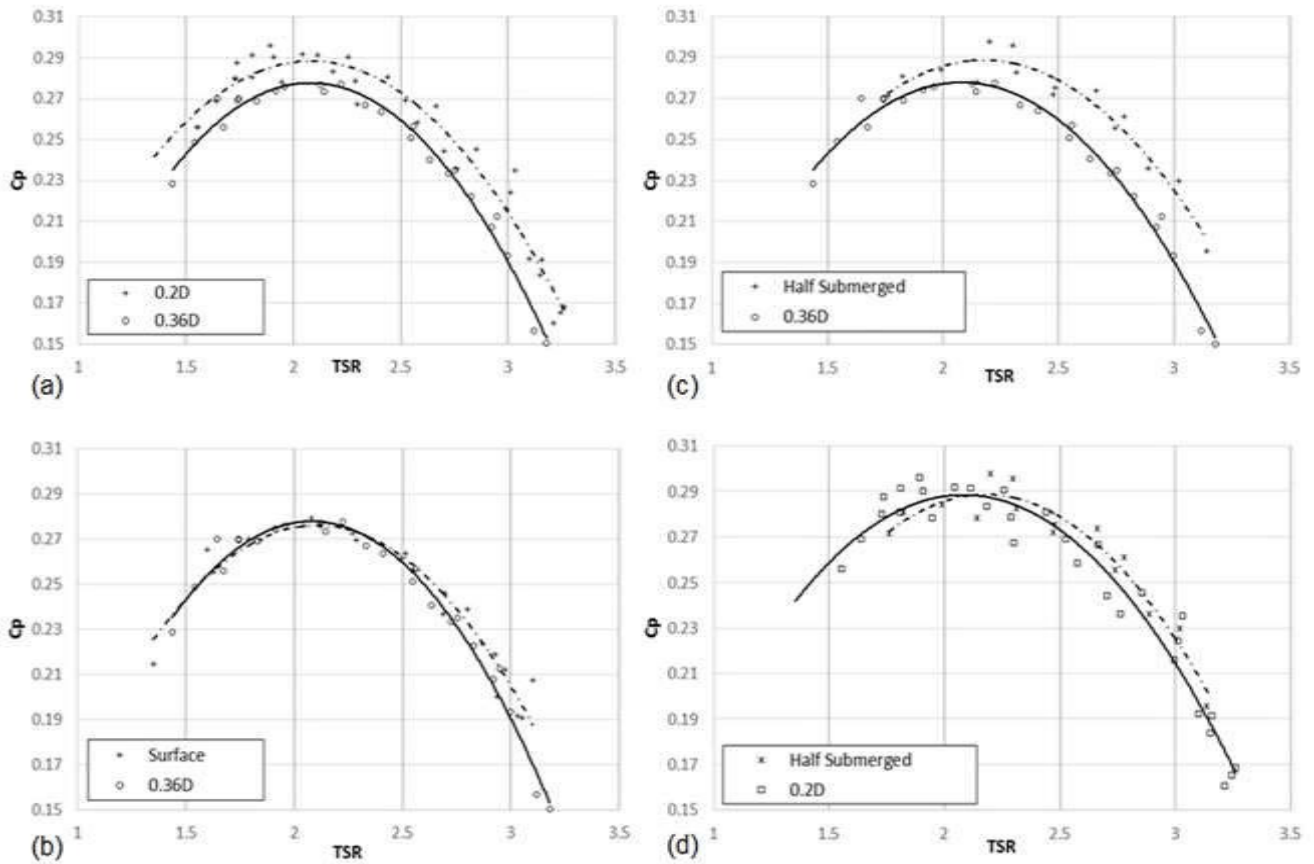
387 The performance of the Hydro-Spinna at shallow immersion and in the half
 388 submerged condition was also compared, as shown in Figure 12(d). The
 389 performances of the Hydro-Spinna in both cases are graphically identical with only a
 390 shift of the tip speed ratio operation in the half submerged case.

391

392 When the turbine is located right below the water surface, the close proximity of the
 393 surface does not affect the performance of the turbine significantly. In the surface
 394 condition, the Hydro-Spinna generated a higher power coefficient at higher TSR than
 395 for the 0.36D case, as shown in Figure 12(b). However, as the turbine is close to the

396 surface, the turbine blade appears to cut through the downstream disturbance from
 397 the front strut generating obvious surface vortices. This effect is more apparent at low
 398 tip speed ratios as the slowly rotating turbine cuts across the disturbances and the
 399 generation of vortices is more prominent.

400



401

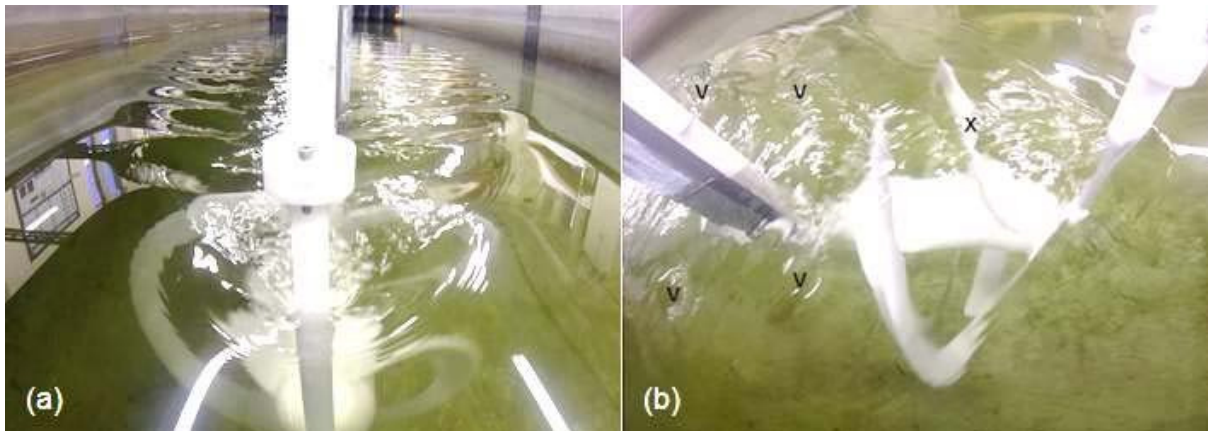
402 Figure 12. The power performance graph of the Hydro-Spinna at different
 403 immersion depths

404

405 It was observed that the front strut seemed to cause more disturbances downstream
 406 to the flow rather than the turbine operation itself and this ultimately disturbed the flow
 407 seen by the turbine, as shown in Figure 13(a). The front strut distorted the unperturbed
 408 profile of the flow approaching the turbine as well as creating a surface wave. In fact
 409 due to their proximity, the turbine in fact saw both the turbulence and downstream
 410 wake of the front strut. As shown in Figure 9(b), as the flow velocity increases and
 411 hence Reynold's Number, the drag coefficient on the whole system also increases.
 412 The turbulence in the flow crucially increased the thrust experienced by the turbine
 413 and overall drag on the system as the flow velocity increases. The combined effect of

414 the front strut wake and rotation of the turbine created vortices on either side of the
415 downstream flow.

416



417

418 Figure 13. The Hydro-Spinna turbine during testing just below the surface condition

419 (a) The wake generated downstream of the system (b) Point X where the turbine
420 cuts across the wake of the front strut creating surface vorticity downstream

421

422 This phenomenon is more obvious with decreasing immersion depth especially at
423 low tip speed ratio. As presented in Figure 13(b), the slowly rotating turbine cut across
424 the wake created by the front strut i.e. point X, creating visible surface vortices on
425 either side of the downstream flow i.e. points V. The power performance of the Hydro-
426 Spinna was affected at low tip speed ratio for the surface condition with the power
427 coefficient being lower than anticipated due to the vortices generated.

428

429 The disturbance caused by the front strut can be minimized by employing a more
430 streamlined profile to reduce the disturbance or even by removing the attachment
431 entirely. However, an installation of the turbine in practice would potentially require a
432 similar arrangement and therefore the experimental results are representative of the
433 operation of the turbine in a real situation. As it may be considered as an integral part
434 of the system, even in a full scale application, the effect of the front strut on the
435 performance of the Hydro-Spinna could be investigated in the future.

436

437 The increased performance of the Hydro-Spinna with decreasing immersion depth
438 presents a unique result as conventional horizontal axis tidal current turbines produce
439 lower power coefficient as the immersion depth reduces [9,14]. Furthermore, the

440 Hydro-Spinna is found to be operable in the half submerged condition. Not only does
441 the Hydro-Spinna performance improve with decreasing depth of immersion, but its
442 ability to generate power under such conditions merits further investigation of the flow
443 profile across the turbine as well as the wake profile downstream of the turbine. The
444 immediate practical implications of the above findings can be the potential of near
445 surface or in surface locations of such devices that could offer huge savings in terms
446 of logistics and maintenance related costs.

447

448 **5. Conclusions**

449 A novel horizontal axis tidal current turbine called “*Hydro-Spinna*”, was introduced
450 and its operations and performance were investigated based on the scaled model tests
451 conducted in the Newcastle University towing tank. The new concept turbine has
452 interesting features including its adaptability to operate in shallow waters and even in
453 partially submerged conditions. The model tests were aimed at investigating the power
454 performance of the Hydro-Spinna at different immersion depths as well as to collect
455 data to support computational modelling for developing the concept further.

456

457 Based on the investigations it was found that:

458

- 459 • The power coefficient of the current model Hydro-Spinna varied between
460 0.275 and 0.3 at an optimum TSR of 2.2 for the deeply submerged condition
461 and shallow submerged condition, respectively. These values are low
462 compared to the power coefficient of typical conventional horizontal axis
463 turbines (HAT).
- 464 • However, in contrast to conventional HATs, the power coefficient of the
465 Hydro-Spinna displayed an increasing trend with decreasing depth of
466 submergence. It was also interesting to note that the turbine can operate at
467 a partially submerged condition with a power coefficient higher than in the
468 fully submerged condition.
- 469 • The drag forces acting on the Hydro-Spinna also displayed an opposite
470 trend to the drag characteristics observed with conventional HATs. As the
471 TSR increased the drag force coefficients were reduced.

- 472 • The maximum power coefficients were observed at lower TSR (e.g. around
473 2.2) as opposed to typically higher TSR values for conventional HATs
474 • Optimal operations at smaller TSRs and hence rotational speeds suggest
475 remote risk of cavitation and the associated undesirable effects of blade
476 erosion and underwater radiated noise
477 • The Hydro-Spinna also displayed earlier starting characteristics compared
478 to typically higher values of conventional HAT's
479 • Despite relatively lower power coefficients, which can be increased further
480 by numerical optimization, the Hydro-Spinna concept may offer greater
481 flexibility for operations at shallower water depths and even in free surface
482 conditions and hence provides improved prospects for logistic and
483 maintenance cost savings in addition to the easy starting of the device and
484 potentially low impact on marine environment.

485

486 Acknowledgements

487 Authors would like to thank Michael Gilbert the designer of the Hydro-Spinna for his
488 contribution to this work. The first author would also like to thank the Brunei
489 Darussalam High Commission for funding her study.

490

491

492 References

- 493 [1] EMEC. European Marine Energy Centre 2013;2013.
494 <http://www.emec.org.uk/marine-energy/tidal-devices/> (accessed March 1,
495 2015).
- 496 [2] Baker A. Tidal Power. Peter Peregrinus Ltd; 1991.
- 497 [3] Fraenkel PL. Marine current turbines: pioneering the development of marine
498 kinetic energy converters. Proc Inst Mech Eng Part A J Power Energy
499 2007;221:159–69. doi:10.1243/09576509JPE307.
- 500 [4] Aly H. State of the art for tidal currents electric energy resources 2011:1119–
501 24.
- 502 [5] Charlier RH. A “sleeper” awakes: tidal current power. Renew Sustain Energy
503 Rev 2003;7:515–29. doi:10.1016/S1364-0321(03)00079-0.

- 504 [6] Hansen MOL. *Aerodynamics of Wind Turbines*. Second. London: Earthscan;
505 2008.
- 506 [7] Lepper PA. Significance of dynamic variation in renewable energy device
507 noise to background noise levels under varying conditions 2014:2–5.
- 508 [8] Wang D, Atlar M, Sampson R. An experimental investigation on cavitation,
509 noise, and slipstream characteristics of ocean stream turbines. *Proc Inst Mech*
510 *Eng Part A J Power Energy* 2007;221:219–31. doi:10.1243/09576509jpe310.
- 511 [9] Bahaj AS, Molland AF, Chaplin JR, Batten WMJ. Power and thrust
512 measurements of marine current turbines under various hydrodynamic flow
513 conditions in a cavitation tunnel and a towing tank. *Renew Energy*
514 2007;32:407–26. doi:10.1016/j.renene.2006.01.012.
- 515 [10] Birjandi AH, Bibeau EL, Chatoorgoon V, Kumar A. Power measurement of
516 hydrokinetic turbines with free-surface and blockage effect. *Ocean Eng*
517 2013;69:9–17. doi:10.1016/j.oceaneng.2013.05.023.
- 518 [11] Bryden IG, Couch SJ. How much energy can be extracted from moving water
519 with a free surface: A question of importance in the field of tidal current
520 energy? *Renew Energy* 2007;32:1961–6. doi:10.1016/j.renene.2006.11.006.
- 521 [12] SeaGen Tidal Technology 2013;2013. <http://www.seageneration.co.uk/>.
- 522 [13] Myers L, Bahaj AS. Wake studies of a 1/30th scale horizontal axis marine
523 current turbine. *Ocean Eng* 2007;34:758–62.
524 doi:10.1016/j.oceaneng.2006.04.013.
- 525 [14] Myers L, Bahaj AS. Power output performance characteristics of a horizontal
526 axis marine current turbine. *Renew Energy* 2006;31:197–208.
527 doi:10.1016/j.renene.2005.08.022.
- 528 [15] Bahaj AS, Myers LE, Rawlinson-Smith RI, Thomson M. The Effect of Boundary
529 Proximity Upon the Wake Structure of Horizontal Axis Marine Current
530 Turbines. *J Offshore Mech Arct Eng* 2012;134:021104.
531 doi:10.1115/1.4004523.
- 532 [16] Li Y, Calışal SM. Modeling of twin-turbine systems with vertical axis tidal
533 current turbines: Part I—Power output. *Ocean Eng* 2010;37:627–37.
534 doi:10.1016/j.oceaneng.2010.01.006.
- 535 [17] Kiho S, Shiono M, Suzuki K. The Power Generation From Tidal Currents by
536 Darrieus Turbine. *Renew Energy* 1996;9:1242–5.
- 537 [18] Yang B, Lawn C. Fluid dynamic performance of a vertical axis turbine for tidal
538 currents. *Renew Energy* 2011;36:3355–66. doi:10.1016/j.renene.2011.05.014.

- 539 [19] Davila-Vilchis JM, Mishra RS. Performance of a hydrokinetic energy system
540 using an axial-flux permanent magnet generator. *Energy* 2013:1–8.
541 doi:10.1016/j.energy.2013.11.040.
- 542 [20] Lin H. Evaluating the performance of an Innovative Marine Current Turbine
543 based on “Wind Spinner” Concept. Newcastle University, 2009.
- 544 [21] Wen Y. Optimisation and Experimental Validation of a Novel Marine Turbine
545 Device , MSc in Marine Engineering 2011.
- 546 [22] Atlar M. Recent upgrading of marine testing facilities at Newcastle University.
547 2nd Int. Conf. Adv. Model Meas. Technol. EU Marit. Ind., 2011, p. 1–32.
- 548 [23] Clarke JA, Connor G, Grant AD, Johnstone C. Design and testing of a contra-
549 rotating tidal current turbine 2007;221:171–9. doi:10.1243/09576509JPE296.
- 550 [24] Luznik L, Flack KA, Lust EE, Baxter DP. Hydrodynamic performance of a
551 horizontal axis tidal turbine under steady flow conditions. *Oceans*, Virginia
552 Beach, VA: 2012, p. 1–4.
- 553 [25] Jo C-H, Lee J-H, Rho Y-H, Lee K-H. Performance analysis of a HAT tidal
554 current turbine and wake flow characteristics. *Renew Energy* 2013:1–8.
555 doi:10.1016/j.renene.2013.08.027.
- 556 [26] Batten WMJ, Bahaj AS, Molland AF, Chaplin JR. Experimentally validated
557 numerical method for the hydrodynamic design of horizontal axis tidal turbines.
558 *Ocean Eng* 2007;34:1013–20. doi:10.1016/j.oceaneng.2006.04.008.
- 559 [27] Galloway PW, Myers LE, Bahaj AS. Experimental and Numerical Results of
560 Rotor Power and Thrust of a Tidal Turbine Operating at Yaw and in Waves
561 2011:2246–53. doi:10.3384/ecp110572246.
- 562